Environmental Science Advances

ROYAL SOCIETY OF CHEMISTRY

PAPER

View Article Online
View Journal | View Issue

Open Access Article. Published on 17 September 2025. Downloaded on 1/13/2026 11:39:36 AM.
This article is licensed under a Creative Commons Attribution-NonCommercial 3.0 Unported Licence.

Check for updates

Cite this: *Environ. Sci.: Adv.*, 2025, **4**, 1834

Effect of seasonal variability of aerosols in radiative forcing and Indian summer monsoon rainfall over south Asia during ENSO events

Sakshi Sharma and Arun Chakraborty *

Received 19th May 2025
Accepted 13th August 2025

DOI: 10.1039/d5va00140d

rsc.li/esadvances

The analysis of seventeen years (2001–2017) of satellite and MERRA-2 model data products demonstrates the influence of seasonal variability of aerosols on Indian summer monsoon rainfall and Aerosol Direct Radiative Forcing (ADRF) at the Top of the Atmosphere (TOA) as well as at the Surface (SFC) during El-Niño/Southern Oscillation (ENSO) events over South Asia. In order to understand the ENSO influence, deviations were quantified from normal years to El-Niño (E_{dev}) and La-Niña (L_{dev}) years. This study investigated greater spatial variability of net ADRF at the TOA (−3 to +3 W m^{-2}) and at the SFC (−5 to +6 W m^{-2}) during the JJAS season during El-Niño years over northwest India, Himalayan region and central India compared to La-Niña years. It is interesting to note that the magnitude of ADRF is highly variable during the post-monsoon season at both the SFC and TOA. The radiative forcing at the SFC varies significantly, more than (±) 10 times the mean during pre-monsoon season. An important observation is the negligible deviation of radiative forcing (L_{dev})at the TOA particularly in the post-monsoon season. Moreover, this study also demonstrates and compares the seasonal variability of aerosols with radiative forcing and their effect on summer monsoon rainfall quantification by using a statistical multiple regression model.

Environmental significance

This study investigated the influence of seasonal variability of aerosols on Indian summer monsoon rainfall and Aerosol Direct Radiative Forcing (ADRF) at the Top of the Atmosphere (TOA) and at the Surface (SFC) during El-Niño/Southern Oscillation (ENSO) events over South Asia. Based on our analysis, negligible deviation of radiative forcing was observed at the TOA during the post-monsoon season. This study also focuses on the spatial variability of net ADRF at the TOA (−3 to +3 W m^{-2}) and at the SFC (−5 to +6 W m^{-2}) during the JJAS season during El-Niño years over northwest India, Himalayan region and central India compared to La-Niña years, which impacts monsoon rainfall.

1 Introduction

Recent studies have shown that the world's climate is changing because of ozone-depleting gases, atmospheric aerosols, changes in insolation and land surface properties.[1] Aerosols could directly influence the Earth–atmospheric system's energy balance through scattering and absorption of solar radiation[2–4] and can indirectly implement changes in climatic conditions by interacting with microphysical properties of clouds.[5–11] In addition, several studies have focused on long-term seasonal and monthly aerosol variability in India and other parts of the world.[12–15] Fluctuations in temperature and radiative forcing have been studied in relation to atmospheric aerosols.[16–18] Periodic oscillations of natural and anthropogenic aerosols and their modulations due to changes in meteorological parameters such as winds, rainfall and relative humidity, and long-range transport have been studied over 35 locations in India.[19] The effect of aerosols on the Earth's radiation budget has been examined in many studies by calculating the radiative forcing at top/bottom of the atmosphere and in the atmosphere.[20–24] Several experimental studies have been carried out to understand the sources of aerosols over the Indian sub-continent and adjoining areas; the potential role of long-range transport; and the impact of natural as well as anthropogenic aerosols such as a mineral dust, black carbon, nitrates, sulfate and organic aerosols on the Earth's radiative budget and forcing.[25–29] Dumka *et al.*[30] analysed the latitudinal variation of aerosol optical properties from the Indo-Gangetic Plains (IGP) to the central Himalayas during the pre-monsoon season of 2008 and 2009 and observed significant changes in columnar aerosol radiative forcing and the columnar heating rate using a radiative transfer model that incorporated vertical profiles of aerosols; they also noted large heterogeneity in aerosol radiative forcing and heating rate at altitudes of about 2 to 4 km over the IGP and

Centre for Ocean, River, Atmosphere and Land Sciences (CORAL), Indian Institute of Technology Kharagpur, Kharagpur-721302, India. E-mail: arunc@coral.iitkgp.ac.in

© 2025 The Author(s). Published by the Royal Society of Chemistry

Open Access Article. Published on 17 September 2025. Downloaded on 1/13/2026 11:39:36 AM.
This article is licensed under a Creative Commons Attribution-NonCommercial 3.0 Unported Licence.

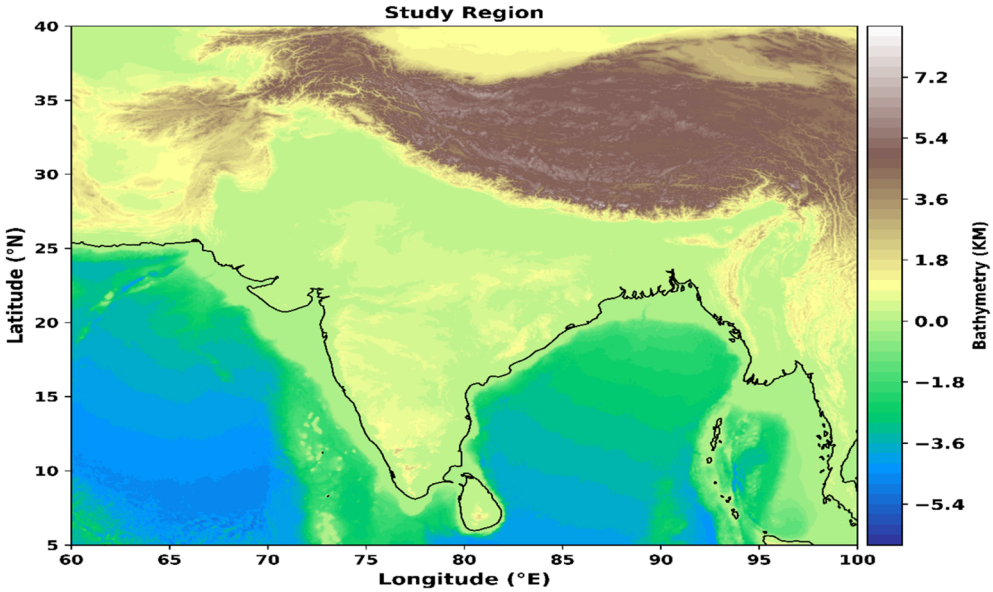

Fig. 1 Study region (5°N–45°N, 60°E–100°E).

central Himalayan region which is an important indicator of the regional climate change and Indian monsoon.

Aerosols are important indicators of changes in weather and climate, which can directly or indirectly affect precipitation. In view of this, Ruchith and Sivakumar[31] clearly explained, with supporting references, that aerosols influence the balance between insolation and terrestrial radiation through their direct absorption and scattering, called "direct effect" or "direct radiative forcing".[32] Several studies have been carried out to characterise the properties and seasonal variability of aerosols as well as their effects such as the aerosol radiative effect or direct radiative forcing and efficiency over many parts of the world. The role of local absorbing aerosols in modulating Indian Summer Monsoon Rainfall (ISMR) has been studied recently. Asutosh and Vinoj[33] showed that mean summer monsoon rainfall is observed over central India and IGP. Strengthening of cyclonic circulation and an increase in convective activity were noted over the Bay of Bengal under a reduced dust scenario.[34] Middey and Panjikkaran[35] showed a negative correlation between sulphate aerosol column mass density and ISMR over central India using long term remote sensing data. The effect of anthropogenic aerosols on the evolution of ISMR has also been studied recently.[36] Investigations on aerosol-El-Niño/Southern Oscillation (ENSO) interactions by Kim *et al.*[37] using the datasets of satellite aerosol measurements and Modern-Era Retrospective Analysis for Research and Applications (MERRA) reanalysis for the period 1979–2011 found a significant relationship between ENSO and aerosol concentration inducing variability in Indian summer monsoon rainfall on seasonal-to-interannual scales. The variability in aerosol properties during ENSO phases was also observed over the tropical Pacific region by using MODIS data for the period 2000–2011.[38] However, studies on aerosol–precipitation interactions during ENSO phases over South Asia are limited. Moreover, the relationship between different aerosols and seasonal precipitation during ENSO phases over India has not yet been studied. Investigation of variability in aerosol–precipitation interactions during ENSO events is of profound importance to understand the regional precipitation changes over South Asia. Therefore, an attempt is made in this present analysis to examine the seasonal variability of aerosols and their possible influence on aerosol direct radiative forcing (ADRF) and precipitation during ENSO events over the South Asian (5°N–40°N; 60°E–100°E) region (Fig. 1).

2 Data and methodology

MERRA-2 model data, Extended Reconstructed Sea Surface Temperature (ERSST) and Satellite datasets are used in this study. SST anomaly values of the Niño 3.4 region (5°S–5°N, 170°W–120°W) were used for identification of ENSO years,[39] based on the criteria of the National Oceanic and Atmospheric Administration (NOAA). The identified El-Niño years (2002, 2009, and 2015), La-Niña years (2007, 2010, and 2011), and normal years (2001, 2003, 2012, and 2013) are considered in our study (Fig. 2). We have used four seasons in this study; December, January and February (DJF) for winter, March April and May (MAM) for pre-monsoon, June, July and August (JJAS) for monsoon, and October and November (ON) for post-monsoon.

2.1 Data

Aerosol column mass density, rainfall and radiative flux datasets were taken from the monthly MERRA-2 Model and the Clouds & the Earth's Radiant Energy System (CERES) products

Open Access Article. Published on 17 September 2025. Downloaded on 1/13/2026 11:39:36 AM.
This article is licensed under a Creative Commons Attribution-NonCommercial 3.0 Unported Licence.

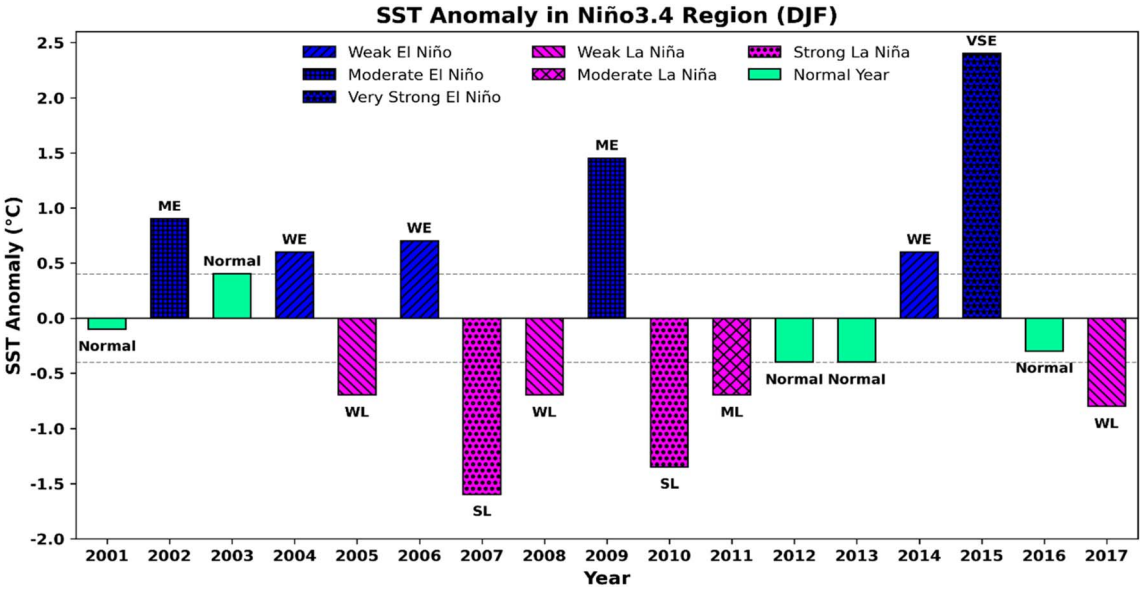

Fig. 2 Three month running mean of Sea Surface Temperature (SST) anomaly values for the Niño 3.4 region (5°S–5°N, 170°W–120°W) for the winter season (DJF). The SST anomaly was calculated by using the Extended Reconstructed Sea Surface Temperature (ERSST)-v4 dataset.[40] ENSO years were identified based on NOAA's criteria. The figure shows that if five constructive overlapping three month mean values are greater than one, then the year is said to be an El-Niño (positive ENSO) year and if less than one, it is considered as a La-Niña (negative ENSO) year.[39]

for the period 2001 to 2017. Further details of the data sets are provided in Table 1.

2.2 Methodology

2.2.1 Aerosol direct radiative forcing (ADRF). The methodology to calculate radiative forcing due to aerosols is described below. Aerosol Direct Radiative Forcing (ADRF) also called Direct Radiative Forcing (DRF) was estimated. Seasonal variability of ADRF was estimated at the top of the atmosphere (TOA) and at the surface (SFC) by using the radiative components of flux (F) data provided for SFC and TOA obtained from the Clouds and the Earth's radiant energy system for the period 2001–2017.

The Shortwave Direct Radiative Forcing (SWADRF), Longwave Direct Radiative Forcing (LWADRF), and Net Direct Radiative Forcing (NET-ADRF) at the TOA are represented in eqn (1)–(3).

$$\mathrm{SWADRF}_{(\mathrm{TOA})} = (F_{(\mathrm{SW}),\ \mathrm{Na}} - F_{(\mathrm{SW}),\ (\mathrm{all\text{-}sky})})_{(\mathrm{TOA})} \quad (1)$$

Table 1 Name of the parameters with product summary and source of the datasets[a]

Sl. No.	Name of the parameters	Data product summary	Source
1	Aerosols column mass density: (black carbon (BC), organic carbon (OC), sulphate (SO_4), dust particles ($PM_{2.5}$) and sea salt aerosols (SS)) (kg m^{-2})	Monthly MERRA-2 model data spatial resolution: 0.5° × 0.625°	https://giovanni.gSFC.nasa.gov/giovanni/
2	Rainfall (mm per month)		
3	Aerosol optical depth (AOD) 550 nm (dark target)	MODIS-Terra monthly data with spatial resolution of 1° × 1°	https://giovanni.gSFC.nasa.gov/giovanni/
4	Radiative flux (W m^{-2}) Variables TOA • SW and LW all-sky total flux • SW and LW all-sky flux with no aerosols SFC • SW and LW all-sky (up/down) total flux • SW and LW all-sky (up/down) flux with no aerosols	Satellite product (terra + aqua edition 4.1). All-sky radiative flux at TOA and surface with and without aerosols. Regional 1° × 1° global grid data.[41]	Clouds and Earth's radiant energy system (CERES) from https://ceres.larc.nasa.gov/products.php?product=SYN1deg
5	Extended reconstructed Sea surface temperature (ERSST)-v4	Spatial resolution 2° × 2°global grid.[42]	https://calcofi.org/about-calcofi/el-ni%C3%B1o-and-la-ni%C3%B1a.html

[a] SW: shortwave, LW: longwave, with no aerosol: Na, TOA: top of the atmosphere, and SFC: surface.

 © 2025 The Author(s). Published by the Royal Society of Chemistry

Open Access Article. Published on 17 September 2025. Downloaded on 1/13/2026 11:39:36 AM.
This article is licensed under a Creative Commons Attribution-NonCommercial 3.0 Unported Licence.

$$\mathrm{LWADRF}_{(\mathrm{TOA})} = (F_{(\mathrm{LW}),\ \mathrm{Na}} - F_{(\mathrm{LW}),\ (\mathrm{all\text{-}sky})})_{(\mathrm{TOA})} \quad (2)$$

$$\mathrm{NET\text{-}ADRF}_{(\mathrm{TOA})} = \mathrm{SWRF}_{(\mathrm{TOA})} + \mathrm{LWADRF}_{(\mathrm{TOA})} \quad (3)$$

where, Na = top of the atmosphere SW/LW flux for the "without aerosol" condition; and all-sky = top of the atmosphere SW/LW flux for the "all sky" condition which includes the presence of aerosols in the atmosphere. The arrow indicates up: ↑, down: ↓.

The direct radiative forcing at the surface can be calculated using the following formulae (eqn (4)–(6)):

$$\mathrm{SWADRF}_{(\mathrm{SFC})} = (F\,(\mathrm{SW}\downarrow - \mathrm{SW}\uparrow)_{(\mathrm{all\text{-}sky})} - F\,(\mathrm{SW}\downarrow - \mathrm{SW}\uparrow)_{\mathrm{Na}})_{(\mathrm{SFC})} \quad (4)$$

$$\mathrm{LWADRF}_{(\mathrm{SFC})} = (F\,(\mathrm{LW}\downarrow - \mathrm{LW}\uparrow)_{(\mathrm{all\text{-}sky})} - F\,(\mathrm{LW}\downarrow - \mathrm{LW}\uparrow)_{\mathrm{Na}})_{(\mathrm{SFC})} \quad (5)$$

$$\mathrm{NET\text{-}ADRF}_{(\mathrm{SFC})} = \mathrm{SWRF}_{(\mathrm{SFC})} + \mathrm{LWADRF}_{(\mathrm{SFC})} \quad (6)$$

2.2.2 Multiple linear regression method. The present analysis also used a statistical multiple linear regression model to examine the relationship between dependent variables (Y) and independent variables (X_i).

$$Y = b_0 + b_1X_1 + b_2X_2 + b_3X_3 + \ldots + b_nX_n \quad (7)$$

where, Y = dependent variable, X_i = independent variable, and b_i = regression coefficients.

We also performed other statistical analyses such as regression coefficients (b_i) with standard error (Std. Error), t-values, P-values, partial correlation coefficients (r_{partial}), and report Variance Inflation Factor (VIF) to understand the robustness of the results. The P-value simply indicates the potential influence of independent parameters on dependent parameters and was used to assess statistical significance, and the P-values are categorised as follows: extremely significant ($^{\#}$): $P < 0.0001$; highly significant ($^{\$}$): $0.0001 \leq P > 0.001$; very significant ($^{+}$): $0.001 \leq P > 0.01$; significant (*): $0.01 \leq P > 0.05$; not significant (^{ns}); $P \geq 0.05$. VIF values indicate the variance inflation factor, with high values representing multicollinearity of the independent variables. Multicollinearity usually arises in a multiple regression model when two or more independent variables are highly linearly related.

3 Results and discussion

Fig. 3 shows the deviation of rainfall variability for the summer monsoon season of June to September (JJAS) during ENSO events with respect to normal years. Fig. 3a and b represent deviations for El-Niño (E_{dev}) and La-Niña (L_{dev}) years JJAS rainfall from Normal years. Fig. 3a indicates a reduction in summer monsoon rainfall during El-Niño years compared to normal years whereas during La-Niña years (Fig. 3b) India experiences more rainfall in the west coastal regions associated with the orographic effect and in north-eastern parts of India. During La-Niña episodes, when the cross-equatorial flow crosses the

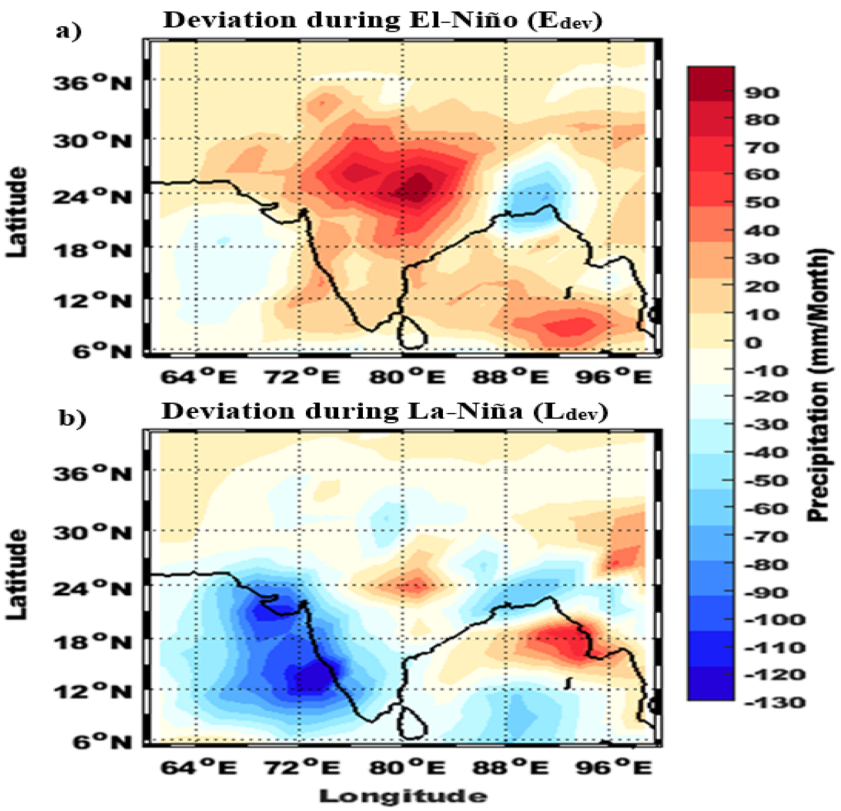

Fig. 3 Deviation of JJAS seasonal precipitation from normal years for (a) El-Niño, and (b) La-Niña event years.

Open Access Article. Published on 17 September 2025. Downloaded on 1/13/2026 11:39:36 AM.
This article is licensed under a Creative Commons Attribution-NonCommercial 3.0 Unported Licence.

equator and enters the Indian landmass, winds are generally stronger over the Somalia coast and Arabian Sea and supply a huge amount of moisture to the Indian continent (moisture from the Indian Ocean and Arabian Sea) particularly in the Southwest monsoon season, which is reduced during El-Niño years due to a weaker pressure gradient between the Mascarene high and the monsoon trough over northeast India. The intensification of the Mascarene High strengthens the cross-equatorial flow in the form of the East African low-level jet.[43] Nevertheless, El-Niño episodes bring rainfall deficits because of cooling and downdraft air over the eastern pole of the Indian Ocean dipole caused by subsequent warm kelvin waves driven by anomalous westerlies, which gradually enhance the growth of El-Niño.[44] Numerous empirical studies have also reported reductions in Indian summer monsoon rainfall (ISMR) due to the developing phase of ENSO.[45–55] ENSO can bring changes in precipitation by creating contrasts in Sea level Pressure (SLP), which leads to changes in dynamical processes of large-scale circulation patterns and surface specific humidity.[31] The influence and importance of dynamical features in modulating the ISMR during ENSO events has been reported.[56] During El-Niño episodes, the monthly mean strength of the Somali Jet is generally (0.4 m s^{-1}) weaker compared with La-Niña episodes. Excess rainfall occurs along the Indian west coast when the monthly mean strength of the Somali Jet is above normal, but deficit rainfall is observed over the west coast of India when the intensity of Somali Jet is below normal. Moreover, precipitation during ENSO events is influenced not only by atmospheric dynamics but also by suspended non-dynamical solid and liquid particles in the atmosphere. So, an attempt is made in this present study to understand the role of non-dynamical parameters (aerosols) in modulating radiative forcing and precipitation during ENSO events.

3.1 Aerosol direct radiative forcing (ADRF) during ENSO events

Dissimilarities in precipitation may be indirectly associated with aerosol radiative forcing. In this present study, the radiation budget measured by aerosol forcing at the surface (SFC) and at the top of the atmosphere (TOA) was calculated by usingeqn (1)–(6). This study analyses the spatial variability of aerosol direct radiative forcing (ADRF) at the TOA and SFC for the four seasons mentioned above over South Asia during ENSO events for the period 2001 to 2017. CERES TOA/SFC shortwave/longwave radiative components of monthly mean all-sky fluxes with and without aerosols were used to calculate ADRF at the TOA and at the SFC. To understand the ENSO influence, deviations were quantified from normal years *i.e.* normal to El-Niño (E_{dev}) and normal to La-Niña years (L_{dev}). Fig. 4a–d and 5a–d depict the seasonal (DJF, MAM, JJAS and ON) spatial variability of NET-ADRF $_{(TOA)}$ (E_{dev}) and NET-ADRF$_{(TOA)}$ (L_{dev}). Fig. 4a and 5a illustrate that during the DJF season, a positive radiative forcing is observed spatially along the Indo-Gangetic Plain (IGP) and slightly over central India in both E_{dev} and L_{dev}.

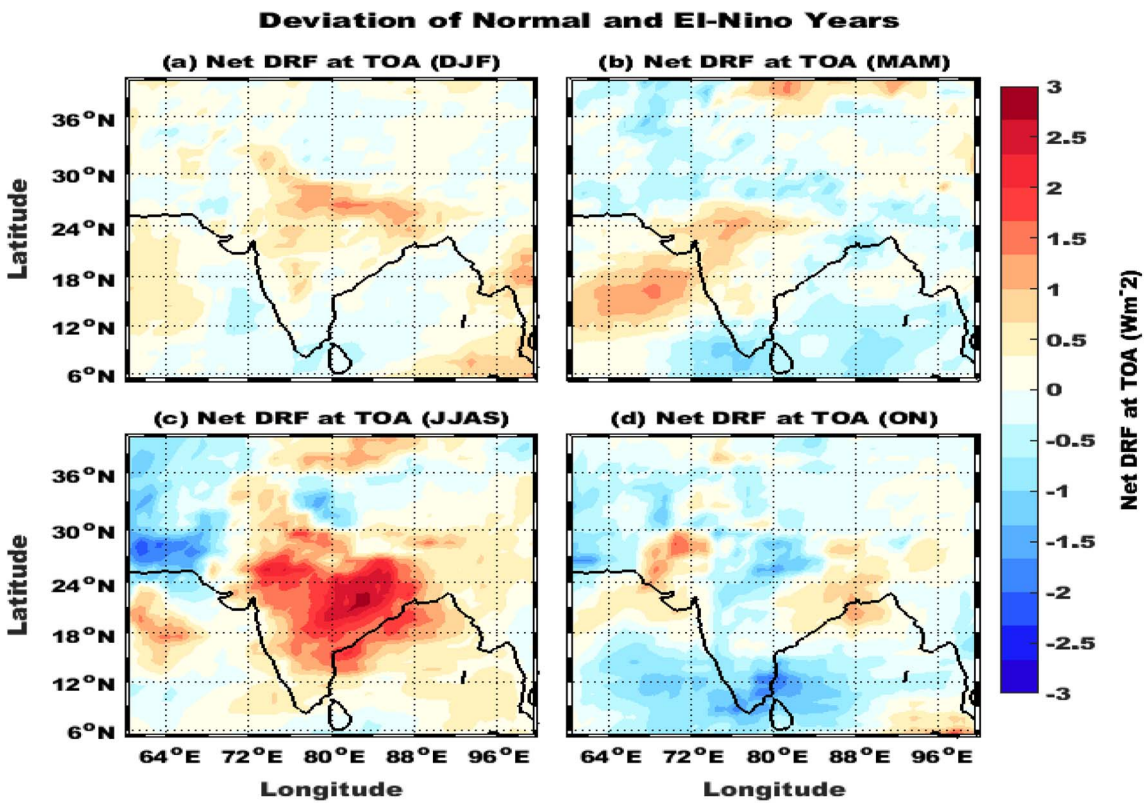

Fig. 4 Seasonal ((a) DJF, (b) MAM, (c) JJAS and, (d) ON) deviations (normal minus El-Niño years) of net aerosol direct radiative forcing at the top of the atmosphere.

 © 2025 The Author(s). Published by the Royal Society of Chemistry

Open Access Article. Published on 17 September 2025. Downloaded on 1/13/2026 11:39:36 AM.
This article is licensed under a Creative Commons Attribution-NonCommercial 3.0 Unported Licence.

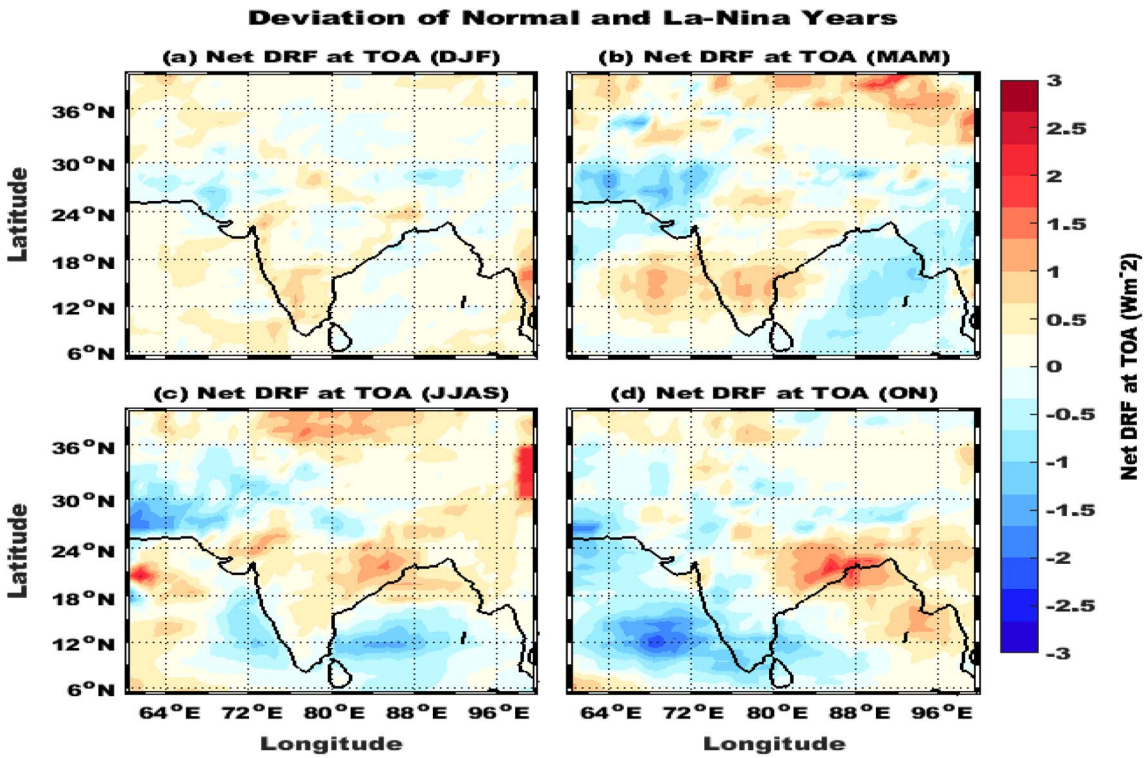

Fig. 5 Seasonal ((a) DJF, (b) MAM, (c) JJAS and, (d) ON) deviations (normal minus La-Niña years) of net aerosol direct radiative forcing at the top of the atmosphere.

But the magnitude of positive radiative forcing is higher in E_{dev} ranging from ~0.5 to 1.5 W m^{-2} than in L_{dev}, where it is less than 0.5 W m^{-2}. During the MAM season, E_{dev} shows positive radiative forcing only over south-eastern Arabian Sea (AS) and central North-west India, while negative radiative forcing is observed over the Bay of Bengal (BOB), south-east Arabian Sea below southern Peninsular India, Pakistan, along the Himalayan region and north-east India and the forcing rate varies between −0.5 and −1.8 W m^{-2}, which represents greater cooling due to outgoing long wave radiation exceeding incoming shortwave radiation. This clearly indicates that cooling induced by aerosols was stronger during the pre-monsoon season of E_{dev} than in L_{dev} (Fig. 4b and 5b). However, in the pre-monsoon season, positive radiative forcing at TOA was observed in L_{dev} over northern Tibetan plateau, central India, central Peninsular India and AS, but among all these regions the highest positive values were observed over Siberian high (Fig. 5b), indicating increased warming over that region due to incoming shortwave radiation exceeding outgoing long wave radiation also called the warming effect, hence strengthening the summer monsoon rainfall owing to establishment of a strong thermal contrast which further promotes strong moisture laden winds. The thermal contrast is induced directly through positive/negative or warming/cooling over the South Asian land mass and adjoining oceans. Warming/cooling during winter and pre-monsoon seasons likely implies the potential strength of summer monsoon rainfall during ENSO events. However, less warming and a low contrast in positive/negative E_{dev} during the winter and pre-monsoon seasons clearly correspond to deficit summer monsoon rainfall during El-Niño years. Fig. 4c and 5c show contradictory spatial variability in the ascertained radiative forcing during the JJAS season for both E_{dev} and L_{dev}.

Enhanced warming was identified only over South Asia, specifically encompassing north-west India (Thar Desert), the Himalayan region, northeast of central India and along the East coast of India; this warming is perhaps due to positive forcing or absorption of insolation by non-rainy polluted clouds while cooling was observed over central and southern BOB and warming rate at TOA for E_{dev} ranged from ~1.5 to 3 W m^{-2} (Fig. 4c). In contrast, warming was absent over the same regions, but cooling was found over central BOB and over central-eastern Arabian Sea (along West coast India) during L_{dev} (Fig. 5c). Whereas, in the ON season, ADRF at TOA for E_{dev} shows cooling extending from central BOB to South-central AS as well as over central India and along the west coast of India, but slight warming is observed along the eastern coast of India and in Pakistan regions (Fig. 4d). L_{dev} also shows similar spatial variability as E_{dev}, at the TOA, but the intensity of warming is slightly higher over the eastern coast of India, absent over Pakistan and cooling over the AS is slightly higher than that over BOB (Fig. 5d). Although the seasonal spatial variability of NET-ADRF at the SFC for E_{dev} and L_{dev} appears to be similar to that at the TOA, the degree of warming/cooling or positive/negative radiative forcing is almost double at the SFC when compared with forcing at TOA (Fig. 6a–d and 7a–d) respectively. Fig. 4c and 6c show greater spatial variability in Net-ADRF for E_{dev} at the

Open Access Article. Published on 17 September 2025. Downloaded on 1/13/2026 11:39:36 AM.
This article is licensed under a Creative Commons Attribution-NonCommercial 3.0 Unported Licence.

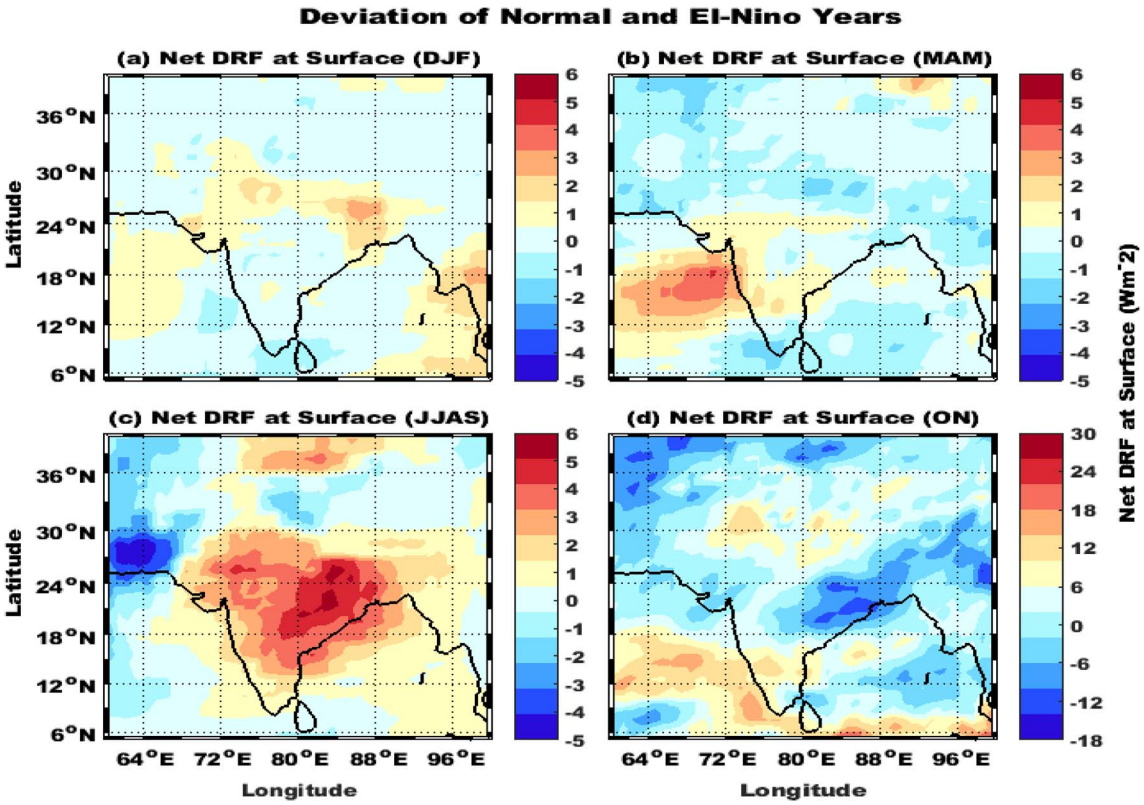

Fig. 6 Seasonal ((a) DJF, (b) MAM, (c) JJAS and, (d) ON) deviations (normal minus El-Niño years) of net aerosol direct radiative forcing at the surface.

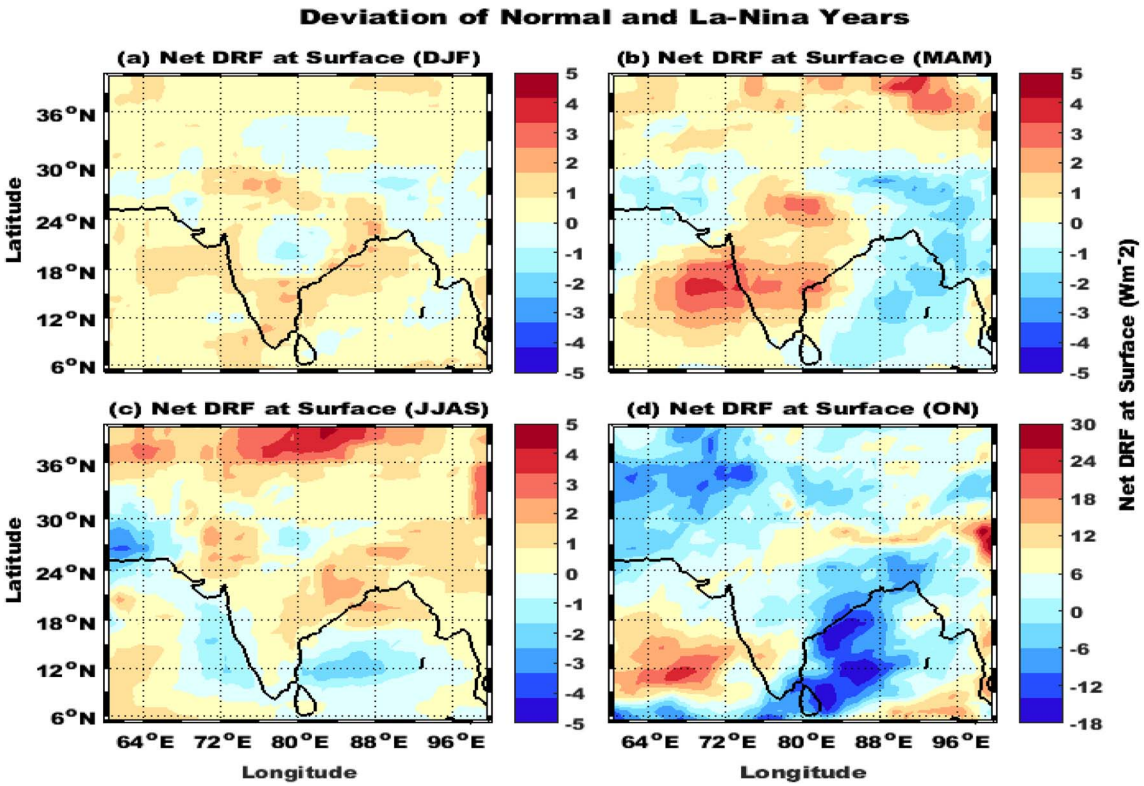

Fig. 7 Seasonal ((a) DJF, (b) MAM, (c) JJAS and, (d) ON) deviations (normal minus La-Niña years) of net aerosol direct radiative forcing at the surface.

 © 2025 The Author(s). Published by the Royal Society of Chemistry

Open Access Article. Published on 17 September 2025. Downloaded on 1/13/2026 11:39:36 AM.
This article is licensed under a Creative Commons Attribution-NonCommercial 3.0 Unported Licence.

TOA and at SFC during the JJAS season over northwest India, the Himalayan region, northeast and central India and the east coast of India compared with other seasons: E_{dev} (−3 to +3 W m^{-2}) and L_{dev} (−5 to +6 W m^{-2}), respectively. It is interesting to note that the magnitude of the NET-ADRF at SFC (−18 to +30 W m^{-2}) is higher during ON seasons for both E_{dev} and L_{dev} (Fig. 7d). Moreover, positive NET-ADRF at the surface and at the top of the atmosphere (Fig. 4c and 6c) owing to a reduction in the summer monsoon rainfall of ∼90 mm $month^{-1}$ during El-Niña when compared with normal years (Fig. 3a), which is due to warming caused by absorbing aerosols at the SFC and TOA during El-Niño episodes. In addition, more positive NET-ADRF at SFC was observed for L_{dev} over the central & eastern Arabian Sea, the west coast of India, and the Siberian High during pre-monsoon, and over the central & eastern parts of India during monsoon, but over the AS during pre-monsoon seasons. Conversely, cooling or negative radiative forcing is observed over Pakistan, northwest India, central & east coast of India and the BOB during the post-monsoon season, and over the BOB and west coast of India during the JJAS season. Most regions during L_{dev} exhibit slight warming and cooling, however, these regions also experienced higher rainfall, ∼130 mm $month^{-1}$ greater during La-Niña years than received in normal years (Fig. 3b).

Seasonal variability of ADRF can be influenced by different types of aerosols such as black carbon (BC), organic carbon (OC), sulphate (SO_4), dust particles ($PM_{2.5}$) and sea salt aerosols (SS) whose physical properties include mass density, scattering, and absorption. Although ENSO does not cause significant changes in seasonal properties of all aerosols, its consequent effects on precipitation are remarkable. The present study also explains the seasonal variability of aerosols and their characteristics during ENSO events over South Asia. This study investigated the seasonal variability of BC, revealing that the column mass density is higher during La-Niña years for all seasons except JJAS, whereas higher values are observed during El-Niño years for JJAS (Fig. 8a). There is no significant difference in ENSO event contributions, but the seasonal variability shows

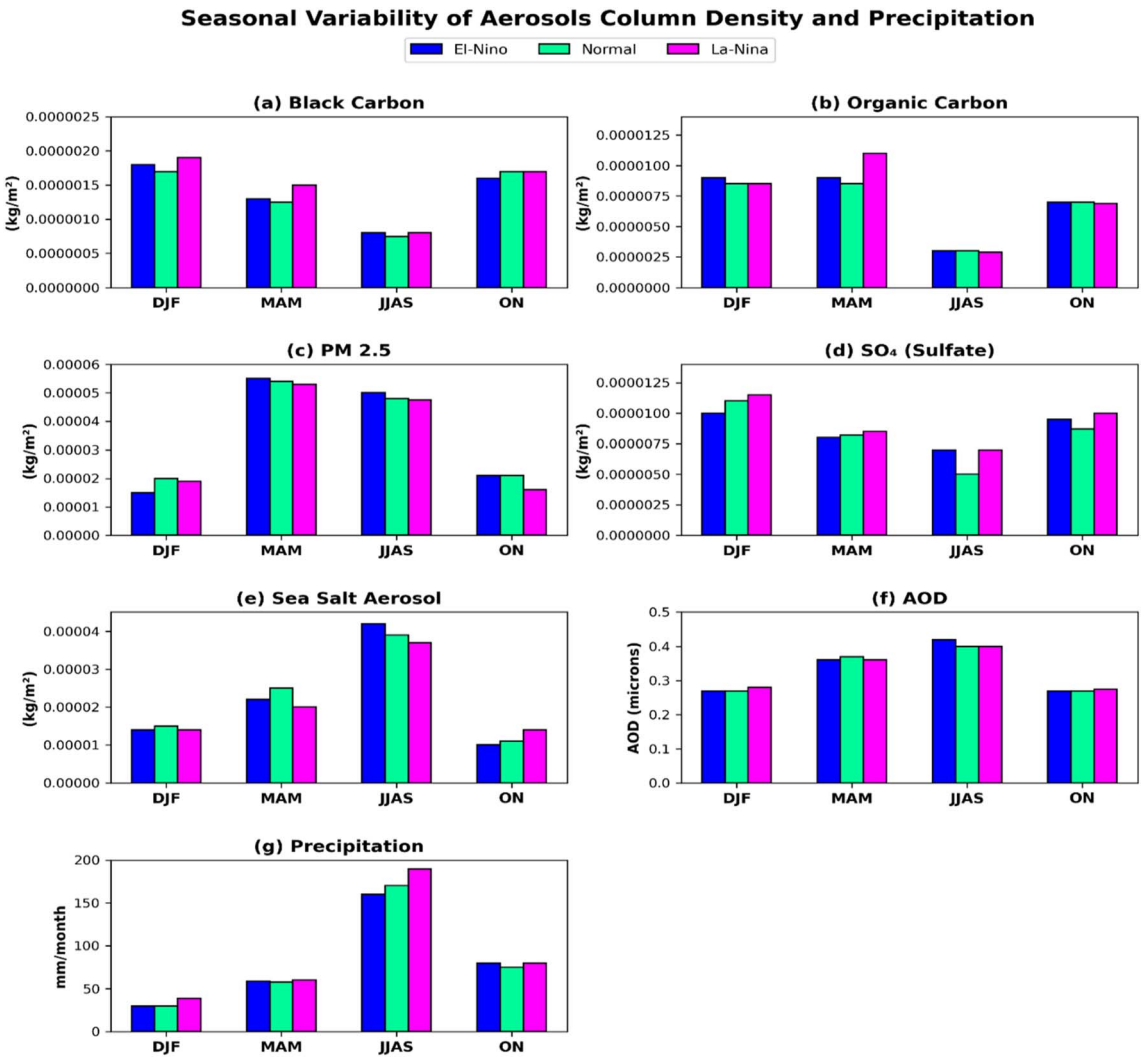

Fig. 8 Seasonal variability of aerosol column mass density of (a) black carbon (BC), (b) organic carbon (OC), (c) particulate matter 2.5 ($PM_{2.5}$), (d) sulfate (SO_4), (e) sea salt aerosol (SS), (f) aerosol optical depth (AOD) and (g) rainfall.

Open Access Article. Published on 17 September 2025. Downloaded on 1/13/2026 11:39:36 AM.
This article is licensed under a Creative Commons Attribution-NonCommercial 3.0 Unported Licence.

notable contrasts. The highest column mass density of BC particles was observed during the winter season, perhaps due to injection of massive anthropogenic aerosols in to the atmosphere through supplementation of anthropogenic sources. Comparatively, very low BC concentrations were observed during the monsoon season than in the pre-monsoon and post-monsoon seasons (Fig. 8a).

A number of studies also revealed that the release of anthropogenic aerosols is higher during early winter (October–November) over the most polluted cities of India due to India's known firework festivals (Diwali, Dusshera, *etc.*), leading to profound degradation of air quality particularly over urban areas such as Delhi,[57] Kolkata,[58] Ahmadabad,[59] and Pune.[60] Nair *et al.*[61] observed the significant role of anthropogenic aerosol sources during winter and the dominance of natural sources during the spring season and they also observed that the difference in aerosol optical depth between these two seasons is small. One of the recent studies by Rana *et al.*[62] provided a detailed explanation of how anthropogenic and natural sources influence seasonal black carbon variability in India by examining the following events namely truck strikes and general strikes, firework events during festivals, intense fog/haze events, forest, grassland and agricultural crop residue burning events and uncontrolled small-scale industrial emissions (brick kilns).

Similarly, the seasonal variability of organic carbon (OC) is comparable to that of black carbon. OC originates primarily from anthropogenic and biogenic sources and is directly released into the atmosphere, which can produce more warming owing to mostly wind-blown mineral dust and other particulates from the earth's crust generally are light absorbing particles. Also OC alters the Earth's radiation budget often through both absorption and scattering. The present study found that the highest column mass density of OC occurs during the pre-monsoon season of both El-Niño and La-Niña episodes. Notably OC concentrations during La-Niña are comparatively higher than during El-Niño. But the opposite is true for the monsoon season (Fig. 8b), which is mainly due to the formation of more 'pre-monsoon bright spots' across many parts of South Asia during Aril-May-June months particularly during El-Niño episodes. In general El-Niño episodes are accompanied by clear skies and low soil moisture, which promote higher temperatures and further lead to severe heat waves and the formation of dry lands during El-Niño years. Dry seasons, such as winter and pre-monsoon seasons, would pile up OC concentrations and transports in to the atmosphere when less moisture and strong winds are present. Clear sky conditions are observed over northwest India, some parts of central–eastern India and southern peninsular India during the winter (Fig. 4a and b) and pre-monsoon (Fig. 6a and b) seasons particularly in El-Niño years. These regions are more frequently affected by heat waves and the formation of drylands over India, which may lead to enhanced OC concentrations during the pre-monsoon season. Few recent studies have reported that the El-Niño episodes are more favourable for the formation of heat waves and drylands under clear sky conditions. Rohini *et al.*[63] analysed gridded temperature data for the period 1961–2013 and reported that the frequency of total duration and maximum duration of heat waves are increasing over central and north-western parts of the India due to the development of anomalous constant high-pressure regions, dominance of anti-cyclonic flow, supplemented with clear skies and depletion of soil moisture. These conditions are likely conducive to the formation of drylands which are responsible for translation of OC components from upper layers of soil to atmosphere or *vice versa*. Laban *et al.*[64] reported that most of the drylands are formed in tropical–temperate areas where the average rainfall is less than the potential moisture loss through evaporation and transpiration. The dryland regions are also considered as key areas for the production, storage and management of carbon stocks. Some renowned organisations have identified high potential drylands as carbon sequestration 'bright spots'. OC concentrations were also found to be higher in the post-monsoon season compared to the summer season perhaps due to relatively dry conditions post-monsoon. This study estimated the sources and sinks of OC based on their production in respective seasons. We found that the winter, pre-monsoon and post-monsoon seasons act like supplementary sources to the atmosphere while most of the organic carbon sinks may occur in wet summers during La-Niña years over South Asia. While, inverse seasonal variations were found between column mass density of $PM_{2.5}$ and SO_4 over south Asia during ENSO events.

$PM_{2.5}$ refers to atmospheric particulate matter (PM), one of the most dangerous pollutants in the atmosphere and its diameter is less than 2.5 micrometers. This can directly affect human health. Rapid growth of population in Indian cities has led to high concentrations of particulates, with both natural and anthropogenic sources contributing significantly. Natural sources are forest and grassland fires, volcanic activity, vegetation and sea salt, whereas, anthropogenic activities include combustion of wood and fossil fuels, running power plants, stubble burning, industrial processes, construction and demolition activities, *etc.* Fig. 8c shows the seasonal variability of $PM_{2.5}$ during ENSO events on the seasonal scale. Relatively higher concentration was observed in the pre-monsoon season than in monsoon season, but a very low concentration was found in both winter and post-monsoon seasons. The highest exceedance of $PM_{2.5}$ occurred during the pre-monsoon season persuaded to organic carbon components from dry upper soil organic matter and lower atmosphere in summer season predominantly from stubble burning. High SO_4 concentration was observed during the winter and post-monsoon seasons, but comparatively low values were observed during the monsoon season than in pre-monsoon seasons. It is interesting to note the strong seasonality of $PM_{2.5}$ during El-Niño episodes across all seasons but enhanced SO_4 concentrations were found during La-Niña episodes in all seasons (Fig. 8d). Yadav *et al.*[65] reported that the contribution of long-range transport of biomass burning aerosol sources plays a significant role during the pre-monsoon and winter seasons. In the pre-monsoon season, transport of polluted air occurs mainly from continental regions of Africa and Middle east due to predominant westerlies. In the post-monsoon season, most of the transport is from the highly polluted Indo-Gangetic Plain (IGP) region, carried by

 © 2025 The Author(s). Published by the Royal Society of Chemistry

Open Access Article. Published on 17 September 2025. Downloaded on 1/13/2026 11:39:36 AM. This article is licensed under a Creative Commons Attribution-NonCommercial 3.0 Unported Licence.

northeasterly winds, and also, they reported that cleaner air masses are transported from Arabian Sea by prevailing south-westerly winds during the monsoon season.

Fig. 8e shows that the production rate of non-light-absorbing sea salt aerosol particles is more during the JJAS season of El-Niño years due to strong south-westerly wind activity which leads to enormous transport from the main source regions of Arabian Sea and South equatorial Indian Ocean to the Indian sub-continent; however the hygroscopic activity of sea salt aerosols is more effective during La-Niña years due to reduced transport. These sea salt aerosols play an important role in modulating the Aerosol Optical Depth (AOD) particularly in the JJAS season. Fig. 8f shows the seasonal mean optical depth of aerosols and higher AOD observed (0.43) observed during the JJAS season of El-Niño compared to normal and La-Niña episodes. AOD is a dimensionless number and certainly gives information about thickness of atmospheric columnar aerosols and how much insolation is prevented from reaching the ground and an AOD value of 0.43 represents that extremely hazy conditions were present during El-Niño episodes, which is mainly due to increased column mass concentration of sea salt aerosols (4.17×10^{-5} kg m^{-2}). Moreover, this study also shows the seasonal variability of rainfall during ENSO events (Fig. 8g).

3.2 Relationship of seasonal aerosols with summer monsoon rainfall during ENSO events

The statistical multiple linear regression model (eqn (7)) had been used to examine the possible effects of seasonal variability of potential predictors such as BC, OC, dust ($PM_{2.5}$), sea salt (SS) aerosols and SO_4 on ADRF and Indian summer monsoon rainfall during ENSO events. This method excludes non-significant parameters with a P value greater than 0.05 and includes a parameter in the model only if its associated significant level is less than 0.05. This analysis showed that during El-Niño years (Table S1), an strong inverse relationship (extremely significant) was observed between JJAS season rainfall and DJF season $PM_{2.5}$ (−0.89) as well as SO_4 (−0.76), while a moderately significant negative relationship was identified with JJAS sea salt aerosol particles (−0.63). Again extremely significant positive relationships with JJAS rainfall were observed for MAM season OC (0.73) and $PM_{2.5}$ (0.65), as well as ON season $PM_{2.5}$ (0.85), SO_4 (0.81) and SS (0.59). This model rejected the seasonal influence of BC; DJF, JJAS and ON season OC as well as the influence of MAM and JJAS season SO_4 and SS during MAM season. It was also observed that the model excluded aerosol parameters during normal years similar to El-Niño years, although the variables included were not statistically significant. An interesting observation during La-Niña years (Table S2) is that almost all seasonal aerosols are included in the model and most of them are significant and a very few parameters excluded from model namely the influence of black carbon during DJF, MAM and ON seasons, and the effect of the sea salt aerosols during the ON season. The results clearly show that the seasonal contribution of aerosols had a stronger influence on summer monsoon rainfall during La-Niña years compared with normal (Table S3) and El-Niño (Table S1) years. The entire model includes aerosol parameters that are correspondingly shown in the active role of summer monsoon rainfall, although some of them have a significant negative role. Certainly, this explains that both seasonal reduction and enhanced magnitude of aerosols would magnify the strength of summer monsoon rainfall. In the present study we observed that the increase in the summer monsoon rainfall during La-Niña years (Table S2) is perhaps due to significant positive effect of sea salt aerosol during DJF (0.35^{+}) & JJAS ($0.44^{\$}$), OC and $PM_{2.5}$ during MAM ($0.67^{\#}$, $0.73^{\#}$) and ON (0.42^{+}, $0.59^{\#}$) as well as BC during JJAS (0.37^{+}). Moreover, a significant negative influence of OC was observed during DJF (-0.22^{ns}) & JJAS (-0.28^{*}), $PM_{2.5}$ during DJF ($-0.51^{\$}$) & JJAS ($-0.63^{\#}$), SO4 during DJF ($-0.37^{+}$), MAM ($-0.25^{ns}$), and JJAS ($-0.42^{+}$), and sea salt aerosols during MAM (-0.23^{ns}) (Table S2).

3.3 Effect of seasonal aerosols and rainfall on aerosol direct radiative forcing (ADRF) at the TOA and SFC during ENSO events

We also examined the effect of seasonal variability of aerosols and rainfall on ADRF at the SFC as well as at the TOA in each respective season of individual ENSO events by using multiple linear regression models. This statistical model clearly demonstrates the essential role of seasonal aerosols (BC, OC, $PM_{2.5}$, SO_4, and SS) and precipitation in radiative forcing. In the El-Niño years, a cooling effect was observed at the SFC and TOA over many parts of South Asian region during DJF season due to the scattering effect of OC, $PM_{2.5}$, and SO_4 (statistically significant) and by sea salt aerosols (statistically not significant), which is represented by a strong negative correlation between these aerosols and NET-ADRF$_{(SFC)}$. But AOD showed a negative influence (statistically significant) on NET-ADRF$_{(TOA)}$ (Table S4). During the MAM season column mass density of almost all aerosols is negatively correlated with NET-ADRF$_{(SFC)}$ except OC, which showed a positive correlation with NET-ADRF$_{(SFC)}$ (Table S4). Only one parameter (SO_4) was excluded from the model along with the precipitation effect. NET-ADRF$_{(TOA)}$ showed significant negative correlation with OC and SO_4, while a positive correlation was observed with BC. This indicates that enhanced warming at the top of the atmosphere over some parts of the South Asia during the pre-monsoon season is perhaps due to enhanced column mass density of BC. During the JJAS season positive and negative NET-ADRF$_{(SFC)}$ are mainly due to BC and $PM_{2.5}$ respectively (Table S4). However, cooling is observed in NET-ADRF$_{(TOA)}$ only due to increased concentrations of the sea salt aerosols (Table S4); although none of the aerosols is included in the model, sea salt aerosols showed significant negative correlation with NET-ADRF$_{(TOA)}$ (99% confidant level). NET-ADRF$_{(SFC)}$ showed a significant positive relationship with AOD and a negative relationship with both BC and SS during the post-monsoon season (ON). But in the ON season, almost all aerosols showed an active role in influencing NET-ADRF$_{(TOA)}$ except SS. Overall across the four seasons of the El-Niño episodes (Table S4), it is clearly observed that the cooling during the winter and post-monsoon seasons was mainly contributed by strong scattering of smaller and brighter aerosol particles such as $PM_{2.5}$, SO_4 and sea salt aerosols. In

Open Access Article. Published on 17 September 2025. Downloaded on 1/13/2026 11:39:36 AM.
This article is licensed under a Creative Commons Attribution-NonCommercial 3.0 Unported Licence.

contrast a warming effect was observed in the winter and pre-monsoon seasons during La-Niña years (Table S5) mainly due to absorption from enhanced surface and atmospheric BC concentrations. Positive ADRF $_{(SFC)}$ during the winter season is due to BC and OC, while in the pre-monsoon season it is due to AOD, SO_4 and SS. This clearly indicates that the gradual increase in surface heating owing to surface level BC and OC during the winter season strengthened the thermal contrast leading to enhanced moisture transport compared to El-Niño years. Table S5 shows that increased SO_4 (0.88^{+}) and SS (0.74^{ns}) concentrations during the pre-monsoon season in the surface and lower atmosphere are associated with increased positive radiative forcing. In addition, BC shows a significant positive effect at the top of the atmosphere during winter, while OC, SS and precipitation show negative correlation with NET-ADRF$_{(TOA)}$. It is also observed that NET-ADRF$_{(TOA)}$ is negatively correlated with AOD, BC and precipitation, but positively correlated with OC, SO_4 and SS during the pre-monsoon season. The influence of SS and precipitation on NET-ADRF$_{(TOA)}$ is observed to be statistically insignificant. During the JJAS season of La-Niña episodes (Table S5), $PM_{2.5}$ and SS show a negative correlation with NET-ADRF$_{(SFC)}$ but at the top of the atmosphere, only two aerosol parameters (BC and AOD) are excluded from the model, while all other aerosols show significant negative relationships, except precipitation which shows a positive relationship with NET-ADRF$_{(TOA)}$, depicting unpolluted brighter clouds with large droplet sizes. It is interesting to note that, ±10 fold greater deviation in NET-ADRF$_{(SFC)}$ and NET-ADRF$_{(TOA)}$ is observed during the ON season during La-Niña episodes because of the active role of all aerosols. The model included all the parameters based on their effective influence on NET-ADRF$_{(SFC)}$ and NET-ADRF$_{(TOA)}$. A significant positive relationship of NET-ADRF is observed with AOD, BC, and precipitation, while a negative relationship is observed with SO_4, SS and OC. The effect of SO_4 is negligible on NET-ADRF $_{(TOA)}$ and hence excluded from model (Table S5).

4 Summary and conclusions

The potential influence of ENSO introduced greater spatial variability in Net ADRF during El-Niño (E_{dev}) both at the TOA and at the SFC during the JJAS season over the northwest, Himalayan region, northeast-central India, and along the East coast of India compared with all the other seasons. The overall variability of E_{dev} and L_{dev} ranges from −3 to +3 W m^{-2} and -5 to +6 W m^{-2} respectively. Warming during the JJAS season (positive ADRF) at the SFC and TOA consequently led to a reduction in Indian summer monsoon rainfall (90 mm month^{-1}) during El-Niño years when compared with normal years, which is due to warming caused by absorbing aerosols at the SFC and TOA during El-Niño episodes. And it is also observed that stronger LW-ADRF occurred during the JJAS season of El-Niño years at both the TOA (−0.065 W m^{-2}) and SFC (−0.1164 W m^{-2}) perhaps due to increased concentrations of aerosol or enhanced column mass density. Conversely, a strong negative ADRF for L_{dev} over the northeast and west coast of India indicates cooling, and hence these regions received high rainfall, ∼130 mm month^{-1} greater amount received during La-Niña years compared to normal years. The influence of ADRF on JJAS precipitation is not only governed by JJAS ADRF but also by the seasonal variability of ADRF during pre-monsoon and post-monsoon. Interestingly, the magnitude of the post-monsoon ADRF for E_{dev} is highly variable at the SFC and TOA. During this season, the spatial variability of maximum radiative forcing reaches ±10 W m^{-2} (Fig. 7d), which is much greater than the mean magnitude (Fig. 8d), while, very small deviations are observed during L_{dev}. Such alterations in insolation and seasonal radiative forcing are mainly due to seasonal variability and different physical properties of various aerosol particles over South Asia.

A reduction in rainfall during El-Niño episodes was accompanied by a high AOD (0.43) representing extremely hazy conditions which was mainly due to the increased column mass concentration of sea salt aerosols; however hygroscopic activity was effective during La-Niña episodes due to reduced transport of sea salt aerosol from the main source regions, Arabian Sea and South equatorial Indian Ocean, to the Indian sub-continent. The column mass density of other aerosols such as BC, OC, dust $PM_{2.5}$ and sulfates was also higher during the JJAS season of El-Niño episodes. Multiple linear regression analysis revealed that, during El-Niño years, a strong inverse relationship was observed between JJAS season rainfall and DJF season SO_4 ($-0.76^{\#}$) and PM 2.5 ($-0.89^{\#}$), while a moderately significant negative relationship was identified with JJAS sea salt aerosol particles ($-0.63^{\#}$), and significant positive relationships were observed with MAM season OC ($0.72^{\#}$) and PM 2.5 ($0.65^{\#}$), as well as with ON season $PM_{2.5}$ ($0.85^{\#}$), SO_4 ($0.81^{\#}$), and SS ($0.59^{\#}$) respectively.

During La-Niña years almost all the seasonal aerosols show significant correlations with JJAS rainfall; however, the influence of black carbon during DJF, MAM and ON seasons, and the effect of sea salt aerosols in the ON season are insignificant. The seasonal contribution of aerosols has a stronger influence on summer monsoon rainfall during La-Niña years compared with normal and El-Niño years. All the aerosol parameters show an active positive role in influencing summer monsoon rainfall, although some of them have a significant negative role. Certainly, this explains that both the seasonal reduction and the enhanced magnitude of aerosols during La-Niña years are favourable for strengthening the summer monsoon rainfall. The cooling effect during the winter and post-monsoon seasons clearly represents the weakening of the summer monsoon rainfall owing to subsistence of a feeble land–sea thermal contrast. The potential strength of summer monsoon rainfall is mainly depends on the buildup of winter and pre-monsoon seasonal humidity, which can be modulated through radiative forcing and the temperature difference between the Indian land mass and surrounding oceans. Moreover, the statistical model also explained that, the warming effect observed in the winter and pre-monsoon seasons of La-Niña years is mainly due to absorption by enhanced surface and atmospheric BC concentrations. However, positive ADRF at the SFC during the winter is due to BC and OC, while in the pre-monsoon season, it is associated with AOD, SO_4 and SS, respectively. This clearly

 © 2025 The Author(s). Published by the Royal Society of Chemistry

Open Access Article. Published on 17 September 2025. Downloaded on 1/13/2026 11:39:36 AM.
This article is licensed under a Creative Commons Attribution-NonCommercial 3.0 Unported Licence.

indicates that the gradual increase in surface heating owing to surface level BC and OC during winter strengthened the thermal contrast and led to a considerable increase in moisture transport during La-Niño years. Whereas, in El-Niño years, the cooling effect observed during the winter and post-monsoon seasons, indicates a weakening of the summer monsoon rainfall.

Author contributions

SS was involved in conceptualization, methodology, software, validation, formal analysis, investigation, resources, data curation, writing – original draft, and visualization. AC contributed to conceptualization, investigation, writing—review, editing, and supervision.

Conflicts of interest

The authors declare no conflict of interest associated with this study.

Data availability

The analysis codes and data can be provided on request.

Supplementary information is available. See DOI: https://doi.org/10.1039/d5va00140d.

Acknowledgements

Sakshi Sharma acknowledges the Ministry of Human Resource and Development (MHRD), Government of India, for the research fellowship. We are grateful to the Indian Institute of Technology Kharagpur for providing the research facilities. The data sources, MODIS, MERRA, NOAA ERSST, and EARTHDATA, are highly acknowledged. We are grateful to the anonymous reviewers for their constructive comments and suggestions, which helped improve the standard of the manuscript.

References

1 C. Papadimas, N. Hatzianastassiou, N. Mihalopoulos, M. Kanakidou, B. D. Katsoulis and I. Vardavas, Assessment of the MODIS Collections C005 and C004 aerosol optical depth products over the Mediterranean basin, *Atmos. Chem. Phys.*, 2009, **9**(9), 2987–2999.

2 T. P. Ackerman and O. B. Toon, Absorption of visible radiation in atmosphere containing mixtures of absorbing and nonabsorbing particles, *Appl. Opt.*, 1981, **20**(20), 3661–3668.

3 R. J. Charlson, S. E. Schwartz, J. M. Hales, R. D. Cess, Jr J. A. Coakley, J. E. Hansen and D. J. Hofmann, Climate forcing by anthropogenic aerosols, *Science*, 1992, **255**(5043), 423–430.

4 J. M. Haywood, V. Ramaswamy and B. J. Soden, Tropospheric aerosol climate forcing in clear-sky satellite observations over the oceans, *Science*, 1999, **283**(5406), 1299–1303.

5 S. Twomey, Atmospheric Aerosols, 1977, pp. 1–316.

6 S. A. Twomey, M. Piepgrass and T. L. Wolfe, An assessment of the impact of pollution on global cloud albedo, *Tellus B*, 1984, **36**(5), 356–366.

7 B. A. Albrecht, Aerosols, cloud microphysics, and fractional cloudiness, *Science*, 1989, **245**(4923), 1227–1230.

8 O. Boucher, S. O. Schwartz, T. P. Ackerman, T. L. Anderson, B. Bergstrom, B. Bonnel, P. Chýlek, A. Dahlback, Y. Fouquart, Q. Fu and R. N. Halthore, Intercomparison of models representing direct shortwave radiative forcing by sulfate aerosols, *J. Geophys. Res.:Atmos.*, 1998, **103**(D14), 16979–16998.

9 A. J. Heymsfield and G. M. McFarquhar, Microphysics of INDOEX clean and polluted trade cumulus clouds, *J. Geophys. Res.:Atmos.*, 2001, **106**(D22), 28653–28673.

10 S. K. Satheesh and K. K. Moorthy, Radiative effects of natural aerosols: A review, *Atmos. Environ.*, 2005, **39**(11), 2089–2110.

11 C. Li, T. Zhao and K. Ying, Effects of anthropogenic aerosols on temperature changes in China during the twentieth century based on CMIP5 models, *Theor. Appl. Climatol.*, 2016, **125**(3), 529–540.

12 R. P. Guleria, J. C. Kuniyal, N. L. Sharma and P. P. Dhyani, Seasonal variability in aerosol optical and physical characteristics estimated using the application of the Ångström formula over Mohal in the northwestern Himalaya, India, *J. Earth Syst. Sci.*, 2012, **121**(3), 697–710.

13 M. I. Mamun, M. Islam and P. K. Mondol, The seasonal variability of aerosol optical depth over Bangladesh based on satellite data and HYSPLIT model, *Am. J. Remote Sens.*, 2014, **2**(4), 20–29.

14 A. Guha, B. Kumar De, P. Dhar, T. Banik, M. Chakraborty, R. Roy, A. Choudhury, M. M. Gogoi, S. Suresh Babu and K. Krishna Moorthy, Seasonal characteristics of aerosol black carbon in relation to long range transport over Tripura in Northeast India, *Aerosol Air Qual. Res.*, 2015, **15**(3), 786–798.

15 M. Kumar, K. S. Parmar, D. B. Kumar, A. Mhawish, D. M. Broday, R. K. Mall and T. Banerjee, Long-term aerosol climatology over Indo-Gangetic Plain: Trend, prediction and potential source fields, *Atmos. Environ.*, 2018, **180**, 37–50.

16 Y. Liu, M. Franklin, R. Kahn and P. Koutrakis, Using aerosol optical thickness to predict ground-level PM2. 5 concentrations in the St. Louis area: a comparison between MISR and MODIS, *Remote Sens. Environ.*, 2007, **107**(1–2), 33–44.

17 R. Gautam, N. C. Hsu, K. M. Lau, S. C. Tsay and M. Kafatos, Enhanced pre-monsoon warming over the Himalayan-Gangetic region from 1979 to 2007, *Geophys. Res. Lett.*, 2009, **36**(7), DOI: 10.1029/2009GL037641.

18 S. Ramachandran and S. Kedia, Black carbon aerosols over an urban region: Radiative forcing and climate impact, *J. Geophys. Res.:Atmos.*, 2010, **115**(D10), DOI: 10.1029/2009JD013560.

19 S. Ramachandran, S. Ghosh, A. Verma and P. K. Panigrahi, Multiscale periodicities in aerosol optical depth over India, *Environ. Res. Lett.*, 2013, **8**(1), 014034.

Open Access Article. Published on 17 September 2025. Downloaded on 1/13/2026 11:39:36 AM.
This article is licensed under a Creative Commons Attribution-NonCommercial 3.0 Unported Licence.

20 S. Verma, C. Venkataraman and O. Boucher, Attribution of aerosol radiative forcing over India during the winter monsoon to emissions from source categories and geographical regions, *Atmos. Environ.*, 2011, **45**(26), 4398–4407.

21 G. A. Pandithurai, R. T. Pinker, T. Takamura and P. C. Devara, Aerosol radiative forcing over a tropical urban site in India, *Geophys. Res. Lett.*, 2004, **31**(12), DOI: 10.1029/2004GL019702.

22 S. Dey, S. Sarkar and R. P. Singh, Comparison of aerosol radiative forcing over the Arabian Sea and the Bay of Bengal, *Adv. Space Res.*, 2004, **33**(7), 1104–1108.

23 D. G. Kaskaoutis, P. R. Sinha, V. Vinoj, P. G. Kosmopoulos, S. N. Tripathi, A. Misra, M. Sharma and R. P. Singh, Aerosol properties and radiative forcing over Kanpur during severe aerosol loading conditions, *Atmos. Environ.*, 2013, **79**, 7–19.

24 C. Sarangi, V. P. Kanawade, S. N. Tripathi, A. Thomas and D. Ganguly, Aerosol-induced intensification of cooling effect of clouds during Indian summer monsoon, *Nat. Commun.*, 2018, **9**(1), 3754.

25 V. C. Ramanathan, P. J. Crutzen, J. T. Kiehl and D. Rosenfeld, Aerosols, climate, and the hydrological cycle, *Science*, 2001, **294**(5549), 2119–2124.

26 K. K. Moorthy, A. Saha, B. S. Prasad, K. Niranjan, D. Jhurry and P. S. Pillai, Aerosol optical depths over peninsular India and adjoining oceans during the INDOEX campaigns: spatial, temporal, and spectral characteristics, *J. Geophys. Res.:Atmos.*, 2001, **106**(D22), 28539–28554.

27 K. K. Moorthy, S. V. Sunilkumar, P. S. Pillai, K. Parameswaran, P. R. Nair, Y. N. Ahmed, K. Ramgopal, K. Narasimhulu, R. R. Reddy, V. Vinoj and S. K. Satheesh, Wintertime spatial characteristics of boundary layer aerosols over peninsular India, *J. Geophys. Res.:Atmos.*, 2005, **110**(D8), DOI: 10.1029/2004JD005520.

28 K. K. Moorthy, S. K. Satheesh, S. S. Babu and C. B. Dutt, Integrated campaign for aerosols, gases and radiation budget (ICARB): an overview, *J. Earth Syst. Sci.*, 2008, **117**(Suppl 1), 243–262.

29 S. Ramachandran, R. Rengarajan, A. Jayaraman, M. M. Sarin and S. K. Das, Aerosol radiative forcing during clear, hazy, and foggy conditions over a continental polluted location in north India, *J. Geophys. Res.:Atmos.*, 2006, **111**(D20), DOI: 10.1029/2006JD007142.

30 U. C. Dumka, N. Tripathi S, A. Misra, D. M. Giles, T. F. Eck, R. Sagar and B. N. Holben, Latitudinal variation of aerosol properties from Indo-Gangetic plain to central Himalayan foothills during TIGERZ campaign, *J. Geophys. Res.:Atmos.*, 2014, **119**(8), 4750–4769.

31 R. D. Ruchith and V. Sivakumar, Influence of aerosol-cloud interaction on austral summer precipitation over Southern Africa during ENSO events, *Atmos. Res.*, 2018, **202**, 1–9.

32 V. C. Ramanathan, P. J. Crutzen, J. T. Kiehl and D. Rosenfeld, Aerosols, climate, and the hydrological cycle, *Science*, 2001, **294**(5549), 2119–2124.

33 A. Asutosh and V. Vinoj, Role of local absorbing aerosols in modulating Indian summer monsoon rainfall, *Sci. Total Environ.*, 2024, **910**, 168663.

34 S. Debnath, G. Govardhan, S. K. Saha, A. Hazra, S. Pohkrel, C. Jena, R. Kumar and S. D. Ghude, Impact of dust aerosols on the Indian Summer Monsoon Rainfall on intra-seasonal time-scale, *Atmos. Environ.*, 2023, **305**, 119802.

35 A. Middey and A. J. Panjikkaran, Effect of Atmospheric Sulphate Aerosol on Precipitation over Central India: A Long-Term Evaluation Through Remote Sensing, *Remote Sens Earth Syst Sci.*, 2025, **22**, 1–7.

36 K. T. Huang, C. H. Sui, M. H. Lo, Y. Y. Kuo and C. W. Chang, Effects of anthropogenic aerosols on the evolution of Indian summer monsoon, *Terr. Atmos. Ocean.*, 2023, **34**(1), 10.

37 M. K. Kim, W. K. Lau, K. M. Kim, J. Sang, Y. H. Kim and W. S. Lee, Amplification of ENSO effects on Indian summer monsoon by absorbing aerosols, *Clim. Dyn.*, 2016, **46**(7), 2657–2671.

38 J. Li, B. E. Carlson and A. A. Lacis, El Niño–Southern Oscillation correlated aerosol Ångström exponent anomaly over the tropical Pacific discovered in satellite measurements, *J. Geophys. Res.:Atmos.*, 2011, **116**(D20), DOI: 10.1029/2011JD015733.

39 J. Y. Yu, Y. Zou, S. T. Kim and T. Lee, The changing impact of El Niño on US winter temperatures, *Geophys. Res. Lett.*, 2012, **39**(15), DOI: 10.1029/2012GL052483.

40 B. Huang, V. F. Banzon, E. Freeman, J. Lawrimore, W. Liu, T. C. Peterson, T. M. Smith, P. W. Thorne, S. D. Woodruff and H. M. Zhang, Extended reconstructed sea surface temperature version 4 (ERSST. v4). Part I: Upgrades and intercomparisons, *J. Clim.*, 2015, **28**(3), 911–930.

41 B. V. Thampi and R. Roca, Investigation of negative cloud radiative forcing over the Indian subcontinent and adjacent oceans during the summer monsoon season, *Atmos. Chem. Phys.*, 2014, **14**(13), 6739–6758.

42 B. Huang, V. F. Banzon, E. Freeman, J. Lawrimore, W. Liu, T. C. Peterson, T. M. Smith, P. W. Thorne, S. D. Woodruff and H. M. Zhang, Extended reconstructed sea surface temperature version 4 (ERSST. v4). Part I: Upgrades and intercomparisons, *J. Clim.*, 2015, **28**(3), 911–930.

43 J. Findlater, Observational aspects of the low-level cross-equatorial jet stream of the western Indian Ocean, *Pure Appl. Geophys.*, 1977, **115**(5), 1251–1262.

44 J. J. Luo, R. Zhang, S. K. Behera, Y. Masumoto, F. F. Jin, R. Lukas and T. Yamagata, Interaction between El Nino and extreme Indian ocean dipole, *J. Clim.*, 2010, **23**(3), 726–742.

45 E. M. Rasmusson and T. H. Carpenter, The relationship between eastern equatorial Pacific sea surface temperatures and rainfall over India and Sri Lanka, *Mon. Weather Rev.*, 1983, **111**(3), 517–528.

46 J. Shukla and D. A. Paolino, The Southern Oscillation and long-range forecasting of the summer monsoon rainfall over India, *Mon. Weather Rev.*, 1983, **111**(9), 1830–1837.

47 D. A. Mooley and B. Parthasarathy, Indian summer monsoon and El Nino, *Pure Appl. Geophys.*, 1983, **121**(2), 339–352.

 © 2025 The Author(s). Published by the Royal Society of Chemistry

Open Access Article. Published on 17 September 2025. Downloaded on 1/13/2026 11:39:36 AM.
This article is licensed under a Creative Commons Attribution-NonCommercial 3.0 Unported Licence.

48 C. F. Ropelewski and M. S. Halpert, Global and regional scale precipitation patterns associated with the El Niño/Southern Oscillation, *Mon. Weather Rev.*, 1987, **115**(8), 1606–1626.
49 R. Kawamura, Mechanism of coupling between the Asian summer monsoon and ENSO, *J. Meteorol.*, 1998, **2**(6), 1009–1027.
50 P. J. Webster and S. Yang, Monsoon and ENSO: Selectively interactive systems, *Q. J. R. Metereol. Soc.*, 1992, **118**(507), 877–926.
51 S. Yang and K. M. Lau, Influences of sea surface temperature and ground wetness onAsian summer monsoon, *J. Clim.*, 1998, **11**(12), 3230–3246.
52 K. Miykoda, A. Navarra and M. N. Ward, Tropical-wide teleconnection and oscillation. II: The enso-monsoon system, *Q. J. R. Metereol. Soc.*, 1999, **125**(560), 2937–2963.
53 N. C. Lau and M. J. Nath, Impact of ENSO on the variability of the Asian–Australian monsoons as simulated in GCM experiments, *J. Clim.*, 2000, **13**(24), 4287–4309.
54 B. Wang, R. Wu and K. M. Lau, Interannual variability of the Asian summer monsoon: Contrasts between the Indian and the western North Pacific–East Asian monsoons, *J. Clim.*, 2001, **14**(20), 4073–4090.
55 B. I. Wang, R. Wu and T. I. Li, Atmosphere–warm ocean interaction and its impacts on Asian–Australian monsoon variation, *J. Clim.*, 2003, **16**(8), 1195–1211.
56 D. Halpern and P. M. Woiceshyn, Somali jet in the Arabian Sea, El Niño, and India rainfall, *J. Clim.*, 2001, **14**(3), 434–441.
57 S. Sarkar, P. S. Khillare, D. S. Jyethi, A. Hasan and M. Parween, Chemical speciation of respirable suspended particulate matter during a major firework festival in India, *J. Hazard. Mater.*, 2010, **184**(1–3), 321–330.
58 A. Chatterjee, S. K. Ghosh, A. Adak, A. K. Singh, P. C. Devara and S. Raha, Effect of dust and anthropogenic aerosols on columnar aerosol optical properties over Darjeeling (2200 m asl), eastern Himalayas, India, *PloS One*, 2012, **7**(7), e40286.
59 S. Ramachandran and T. A. Rajesh, Black carbon aerosol mass concentrations over Ahmedabad, an urban location in western India: comparison with urban sites in Asia, Europe, Canada, and the United States, *J. Geophys. Res.:Atmos.*, 2007, **112**(D6), DOI: 10.1029/2006JD007488.
60 P. C. Devara, M. P. Alam, U. C. Dumka, S. Tiwari and A. K. Srivastava, Anomalous features of black carbon and particulate matter observed over rural station during Diwali festival of 2015, in *Environmental Pollution: Select Proceedings of ICWEES-2016*, Singapore, Springer Singapore, 2017, pp. 293–308.
61 V. S. Nair, S. S. Babu, M. R. Manoj, K. K. Moorthy and M. Chin, Direct radiative effects of aerosols over South Asia from observations and modeling, *Clim. Dyn.*, 2017, **49**(4), 1411–1428.
62 A. Rana, S. Jia and S. Sarkar, Black carbon aerosol in India: a comprehensive review of current status and future prospects, *Atmos. Res.*, 2019, **218**, 207–230.
63 P. Rohini, M. Rajeevan and A. K. Srivastava, On the variability and increasing trends of heat waves over India, *Sci. Rep.*, 2016, **6**(1), 1–9.
64 P. Laban, G. Metternicht and J. Davies, *Soil Biodiversity and Soil Organic Carbon: Keeping Drylands Alive*, Gland, Switzerland, IUCN, 2018, vol. 10.
65 R. Yadav, L. K. Sahu, S. N. Jaaffrey and G. Beig, Temporal variation of particulate matter (PM) and potential sources at an urban site of Udaipur in Western India, *Aerosol Air Qual. Res.*, 2014, **14**(6), 1613–1629.